RESEARCH ARTICLE

JBMR®

Sirt3 Promotes Chondrogenesis, Chondrocyte Mitochondrial Respiration and the Development of High-Fat Diet-Induced Osteoarthritis in Mice

Shouan Zhu,[1,†] Elise L. Donovan,[1,‡] Dawid Makosa,[1,§] Padmaja Mehta-D'souza,[1] Anita Jopkiewicz,[1,¶] Albert Batushansky,[1,||] Dominic Cortassa,[1,**] Aaron D. Simmons,[1,††] Erika Barboza Prado Lopes,[1,‡‡] Michael Kinter,[1] and Timothy M. Griffin[1,2,3]

[1]Aging and Metabolism Research Program, Oklahoma Medical Research Foundation, Oklahoma City, OK, USA
[2]Department of Biochemistry and Molecular Biology, Department of Physiology, Oklahoma Center for Geroscience, University of Oklahoma Health Sciences Center, Oklahoma City, USA
[3]Biomedical Laboratory Research and Development, Veterans Affairs Medical Center, Oklahoma City, USA

ABSTRACT

Understanding how obesity-induced metabolic stress contributes to synovial joint tissue damage is difficult because of the complex role of metabolism in joint development, maintenance, and repair. Chondrocyte mitochondrial dysfunction is implicated in osteoarthritis (OA) pathology, which motivated us to study the mitochondrial deacetylase enzyme sirtuin 3 (*Sirt3*). We hypothesized that combining high-fat-diet (HFD)-induced obesity and cartilage *Sirt3* loss at a young age would impair chondrocyte mitochondrial function, leading to cellular stress and accelerated OA. Instead, we unexpectedly found that depleting cartilage *Sirt3* at 5 weeks of age using *Sirt3-flox* and *Acan*-Cre^{ERT2} mice protected against the development of cartilage degeneration and synovial hyperplasia following 20 weeks of HFD. This protection was associated with increased cartilage glycolysis proteins and reduced mitochondrial fatty acid metabolism proteins. Seahorse-based assays supported a mitochondrial-to-glycolytic shift in chondrocyte metabolism with *Sirt3* deletion. Additional studies with primary murine juvenile chondrocytes under hypoxic and inflammatory conditions showed an increased expression of hypoxia-inducible factor (HIF-1) target genes with *Sirt3* deletion. However, *Sirt3* deletion impaired chondrogenesis using a murine bone marrow stem/stromal cell pellet model, suggesting a context-dependent role of *Sirt3* in cartilage homeostasis. Overall, our data indicate that *Sirt3* coordinates HFD-induced changes in mature chondrocyte metabolism that promote OA. © 2022 The Authors. *Journal of Bone and Mineral Research* published by Wiley Periodicals LLC on behalf of American Society for Bone and Mineral Research (ASBMR).

KEY WORDS: OBESITY; OSTEOARTHRITIS; HIGH-FAT DIET; *Sirt3*; PRIMARY JUVENILE MURINE CHONDROCYTES; METABOLISM

Introduction

Obesity is a major risk factor for osteoarthritis (OA), and there is increasing evidence that metabolic factors independently contribute to OA pathogenesis.[1-3] Within cartilage, previous studies link chondrocyte mitochondrial dysfunction and impaired energy sensor systems (e.g., AMPK and sirtuins) to post-traumatic and age-associated OA.[3-5] However, the extent to which these cellular metabolic factors contribute to obesity-induced OA is not well understood.[6] Prior studies, including our work on high-fat-diet (HFD)-induced OA in mice,[7,8] associated an increase in dietary

Received in original form December 22, 2021; revised form September 9, 2022; accepted October 6, 2022.
Address correspondence to: Timothy M. Griffin, Aging and Metabolism Research Program, MS 21, Oklahoma Medical Research Foundation, Oklahoma City, Oklahoma, 73104, USA.
E-mail: griffint@omrf.org.
Additional Supporting Information may be found in the online version of this article.

Journal of Bone and Mineral Research, Vol. 37, No. 12, December 2022, pp 2531–2547.
Present addresses: †Department of Biomedical Sciences, Ohio Musculoskeletal and Neurological Institute (OMNI), Ohio University, Athens, Ohio, 45701, USA, ‡Department of Human Physiology, Gonzaga University, Spokane, Washington, 99205, USA, §School of Molecular Sciences, Harry Perkins Institute of Medical Research, University of Western Australia, Perth, Western Australia, Australia, ¶Max Planck Institute for Biology of Ageing, Cologne Graduate School of Ageing Research, Joseph-Stelzmann-Str. 9b, 50931, Cologne, Germany, ||Research Support Laboratories at the Ilse Katz Institute, Ben-Gurion University, Be'er-Sheva, Israel, **Boston University Henry M. Goldman School of Dental Medicine, Boston, Massachusetts, 02118, USA, ††Department of Chemical and Biological Engineering, University of Wisconsin-Madison, Madison, Wisconsin, 53706, USA, ‡‡Astellas US LLC, San Francisco, California, 94108, USA
DOI: 10.1002/jbmr.4721

saturated fatty acids (FAs) to OA pathology and chondrocyte stress.[9-11] Furthermore, single-cell RNA-sequencing (scRNA-seq) analysis of cells isolated from osteoarthritic articular cartilage identified seven putative cell clusters, including a novel "effector chondrocyte" population characterized by steroid biosynthesis and FA metabolism.[12] Altered cholesterol metabolism was also recently implicated in OA pathology.[2]

One way in which HFDs cause cellular stress is through post-translational hyperacetylation of mitochondrial proteins.[13,14] The mitochondrial deacetylase enzyme sirtuin 3 (*Sirt3*) regulates the acetylation status of hundreds of mitochondrial proteins, including those regulating FA oxidation such as long-chain acyl-CoA dehydrogenase (ACADL).[13,15] We previously found that aging reduced the cartilage protein content of SIRT3, resulting in hyperacetylation and impaired activity of the mitochondrial antioxidant enzyme SOD2 in F344/BN F1 hybrid rats.[16] Cartilage SIRT3 prot content also declined with age in C57BL/6 mice, and *Sirt3* knock-out (KO) mice developed a modest increase in early OA pathology at 14 months of age.[16,17] Therefore, we hypothesized that combining diet-induced obesity and the loss of *Sirt3* in cartilage at a young age would impair chondrocyte mitochondrial function, leading to cellular stress and accelerated OA pathology.[13,15]

Methods

Additional detailed methods are provided in the supplemental materials.

Animal study design

All animal studies were reviewed and approved by the AAALAC International-accredited Institutional Animal Care and Use Committee at the Oklahoma Medical Research Foundation (OMRF). Mice were group housed in a specific-pathogen-free facility under a controlled environment (22 ± 3°C on 14 h:10 h light/dark cycles) in ventilated cages (≤5 animals/cage) with ad libitum access to chow (Lab Diet 5053) and sterilized water. We tested our hypothesis by conditionally deleting *Sirt3* in the cartilage of mice at 5 weeks of age and then fed mice a control (10% kcal fat; D12450Ji, Research Diets) or HFD (60% kcal fat; D12492i) from 6 to 26 weeks of age (Fig. 1*A*). At 24 weeks of age, body fat was measured by quantitative magnetic resonance (Echo Medical Systems), and glucose tolerance testing was performed as previously described.[8] *Acan-Cre*$^{ERT2(+/-)}$ and *Sirt3-flox*$^{(F/F)}$ mice[18] were bred to generate inducible cartilage deficient mice (iC-Sirt3 KO), with littermate *Acan-Cre*^{ERT2}-null mice used as wild type (WT) controls. *Sirt3-flox* and *Sox2-Cre* mice were bred to produce offspring with a germline loss-of-function mutation in epiblast-derived cells (*Sirt3 KO*) for in vitro experiments. All mice were C57BL/6J background.

Animal experiment sample sizes were based on power analyses for OA histopathology, our primary outcome. Using data from prior studies in our lab, $n = 9$ animals per group was estimated to provide 80% power to detect a 30% difference in mean osteoarthritis research society international (OARSI) murine OA histopathology scores at $p = .05$ (mean OARSI score of 1.0 and standard deviation of 0.2). Primary cell in vitro experiments were conducted on cells collected from a minimum of three animals. For scRNA-seq experiments, cells were either pooled from three animals (Experiment 1) or replicated three times using cells harvested from animals born in three separate litters (Experiment 2). For chondrogenic pellet experiments, cells isolated from each animal were tested in all three culture conditions, allowing for a repeated-measures statistical design. Sample sizes for specific experiments are noted in the figures.

Joint tissue processing and analyses

The left knee joint was processed for semi-quantitative OA histopathology grading, as previously described.[8] Briefly, three coronal sections spaced throughout the load-bearing region were stained with hematoxylin, Fast Green, and safranin-O for blinded grading of cartilage pathology (OARSI scoring), osteophyte pathology, and synovial lining cell hyperplasia. The right knee was used to harvest articular cartilage immediately following death for RNA and protein isolation, as previously described.[8] Briefly, cartilage pieces were frozen at minus 80°C in TRIzol™ (Invitrogen, USA) and then processed to generate approximately 1 μg of RNA with RNA Clean and Concentrator Columns (Zymo Research, USA) per manufacturer's protocol. Protein in the lower organic phase fraction from the TRIzol™ extraction was processed as previously described for mass spectrometry (MS).[8,16] Gene expression was quantified with a targeted Fluidigm DELTA-gene Assay (Table S1) conducted following manufacturer's instructions using a Fluidigm 96.96 Dynamic Array IFC and Biomark HD instrument. RStudio with stats package was used to compute delta-Ct values of target genes by subtracting the geometric mean of Ct values of five reference genes (*Actb*, *B2m*, *Gapdh*, *Gusb*, *Hsp90ab1*). Genotype and diet-specific effects on gene expression were evaluated using log2-transformed volcano plot comparisons and two-factor ANOVA. The abundance of 113 proteins involved in cellular metabolism and redox homeostasis was quantified using MS selective reaction monitoring (SRM), as previously reported.[8,16] The geomean of two protein-specific peptide areas was used for protein quantification normalized to a bovine serum albumin (BSA) internal standard to determine the abundance. Femoral head (hip) cartilage was isolated from 5-week-old WT and *Sirt3 KO* mice immediately following death for gas chromatography (GC)–MS semi-targeted metabolic profiling, as previously described.[19] Cartilage was pooled from four animals per biological replicate, and five biological replicates were measured for each genotype. Metabolite relative abundance was calculated by peak area normalized to sample wet weight and internal standard (ribitol).[19]

Primary chondrocyte isolation and in vitro assays

Primary immature chondrocytes were isolated from knee epiphyseal cartilage of 6- to 8-day-old mice following a previously published protocol.[20] Cells were expanded in complete DMEM medium (Life Technology, 10567014) supplemented with 10% fetal bovine serum (FBS) and 1% penicillin/streptomycin (P/S). Cells were reseeded for Seahorse-based metabolism assays, in vitro stimulation experiments, or comparative scRNA-seq analyses. Seahorse assays were conducted as previously described[21] using an XFe24 Analyzer (Agilent). Glycolytic rate and mitochondrial stress assays were performed following manufacturer's instructions, with WT and *Sirt3 KO* cells tested in duplicate on the same plate (duplicate values averaged). Cells were harvested from eight to 15 animals per genotype, which were generated from ≥3 litters per genotype. Data were normalized to cell number. In vitro stimulation experiments were conducted on passage 1 cells isolated from WT and *Sirt3 KO* animals and challenged under three culture conditions: hypoxia (1% for 48 hours), interleukin-1β (IL-1β) (10 ng/mL for 24 hours; R&D Systems, #401-ML), and FAs (0.5 mM of 1:1 oleate:palmitate for

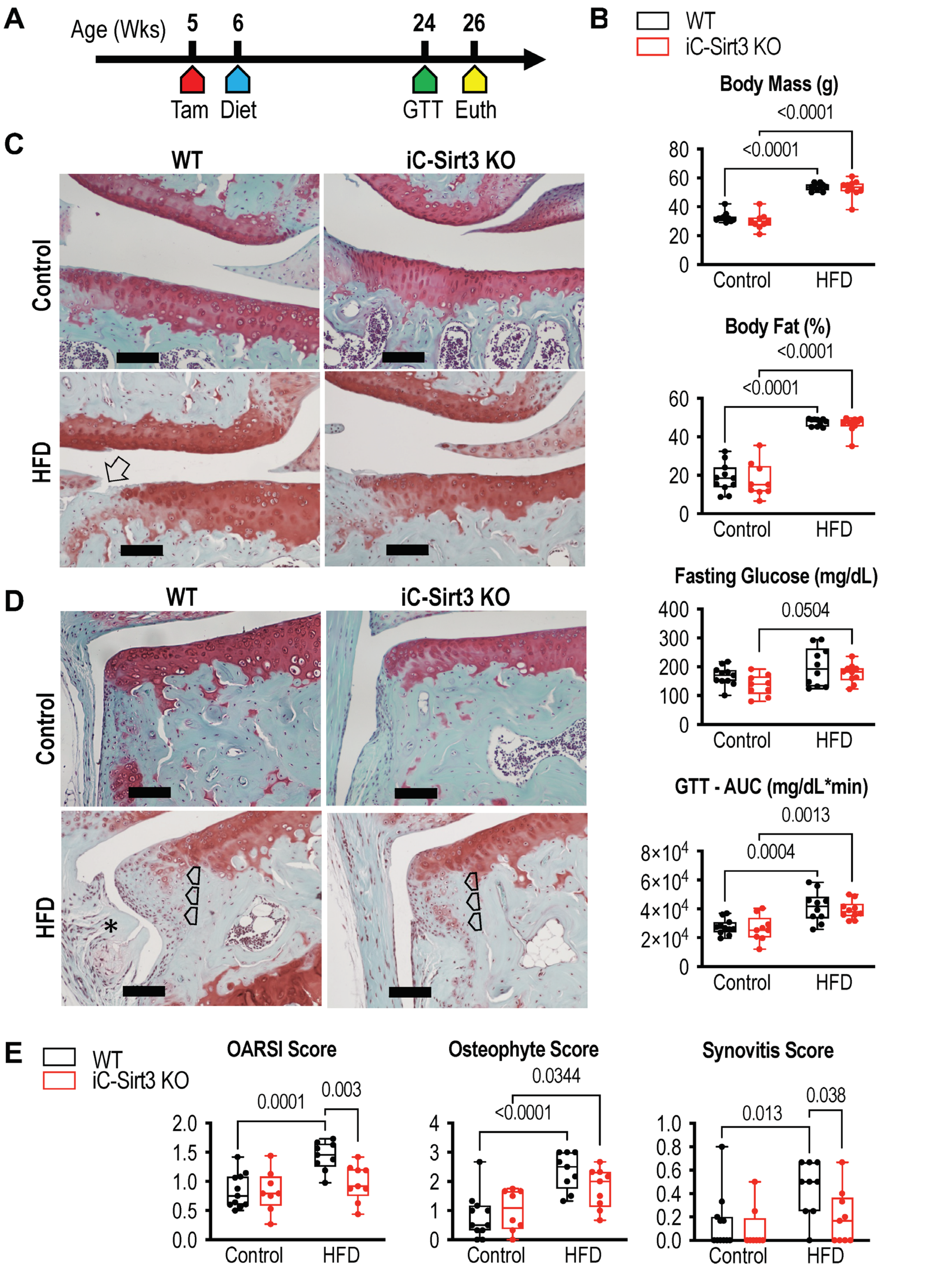

(Figure legend continues on next page.)

24 hours). Experiments were evaluated by gene expression using previously described targeted Fluidigm DELTAgene Assay.

For scRNA-seq experiments, cells were isolated from littermate 8-day-old ($n = 3$) WT mice and expanded to approximately 90% confluency over 7 days. Cells were released with Trypsin–EDTA, and a single-cell suspension in 1X PBS with 1% BSA was added to one well of the 10× chromium controller (10× Genomics, Pleasanton, CA). A detailed description of the method is provided in the supplemental materials. For the comparative scRNA-Seq analysis between WT and *Sirt3 KO* cells, cryopreserved chondrocytes were used from three separate litters per genotype. Two days prior to the scRNA-seq experiments, one frozen cell pellet of each genotype and sex (WT-M, WT-F, KO-M, KO-F) was thawed and expanded in six-well culture plates. Cells were prepared essentially as previously described, except for being released with Accutase. In addition, each sample was labeled with a unique oligo hashtag (details in supplemental methods) to enable pooling samples of each genotype and sex before adding them to a single well of the 10× chromium controller. This was repeated three times for the final comparative scRNA-Seq data set.

Single-cell capture, RNA sequencing, data analysis, and visualization

Cell capture, cDNA generation, and library preparation were performed using a Chromium Single Cell 3′ v3 reagent kit following the manufacturer's instructions. The scRNA-seq library was run on an Illumina NovaSeq S1 (initial WT analysis) or Illumina NovaSeq S4 (comparative analysis). Cell Ranger software was used to demultiplex samples, process barcodes, align to the mouse (GRCm38/mm10) genome assembly, and count single-cell genes. For analyzing data obtained from cultured chondrocytes pooled from three WT mice, the count matrix was imported into RStudio, and subsequent analysis was performed using the Seurat 3.2 package. For the comparative analysis between WT and *Sirt3 KO* cryopreserved chondrocytes, the count matrices from Cell Ranger were imported into Partek® Flow® software, version 10.0. After filtering based on quality assurance/quality control parameters (Fig. S3), data were log2-normalized and scaled. Highly variable features were selected by applying a variance stabilizing transformation (*vst*), and the top 2000 of these features were selected for downstream analyses. Dimensionality reduction was performed using principal component analysis (PCA), and an Elbow plot (in R Studio) or a Scree plot (in Partek® Flow®) was used to determine the dimensionality of the data set. A graph-based clustering approach (K-nearest-neighbor) was used to cluster the cells, which were visualized by Uniform Manifold Approximation and Projection (UMAP). Differentially expressed genes (≥1.5-fold change or log2_Fc threshold ≥ 0.6) with 5% false discovery rate (FDR)-corrected significance (qFDR < 0.05) were determined by cluster or by genotype and cluster for the comparative analysis. Predicted biological processes associated with over- or underrepresented differentially expressed genes were evaluated using gene ontology enrichment analysis.

Bone marrow stem/stromal cell isolation and cartilage pellet culture model

Bone marrow stem/stromal cells (BMSCs) were isolated from the hindlimbs of 6-week-old C57BL6J mice. A single-cell suspension of BMSCs was cultured in DMEM with 10% FBS and 1% P/S, and only cells that adhered after 3 hours were maintained with periodic changes of fresh medium. Cultured BMSCs were then characterized by flow cytometry and evaluated for multipotency using adipocyte, osteocyte, and chondrocyte assays (Fig. S5). To generate cartilage pellets, BMSCs from WT and *Sirt3 KO* mice were transferred to MesenCult™-ACF Chondrogenic Differentiation Medium (STEMCELL Technologies, #05455) with or without 1% BSA or 0.5 mM FA. Pellets were collected after 3–28 days of differentiation. Pellet images were captured with a stereomicroscope (Nikon SMZ800), and paraffin-embedded sections were stained with safranin-O (Fig. S6). Sections were also immunostained with antibodies for COL2 (abcam, ab185430), PRG4 (Millipore, AB2200), SIRT3 (Cell Signaling Technology, 5490), and perilipin (Cell Signaling Technology, 3470). Staining intensity and distribution throughout the pellet were quantified by Zeiss Zen software (Fig. S7). For each experiment, BMSCs were collected from separate animals to generate three biologically independent pellets ($n = 3$) tested in each treatment group per time point.

Statistical analyses

Genotype and diet effects were evaluated by two-way ANOVA. Data that did not meet test assumptions for homoscedasticity, even after log transformation, were analyzed by Kruskal–Wallis or Mann–Whitney tests. Tests showing a significant effect of diet or genotype ($p < .05$) were followed up with multiple-comparison post hoc tests to identify individual group differences as specified in figure legends. Differential gene expression analyses were based on two-tailed Student's t test of log2-transformed data, with significance set at 1.5-fold change

(Figure legend continued from previous page.)

Fig. 1. Inducible cartilage deletion of *Sirt3* (iC-Sirt3 KO) prevented the development of high-fat-diet (HFD)-induced cartilage pathology and synovitis in male mice. (*A*) Mice were administered tamoxifen at 5 weeks of age and then fed either a defined control diet (10% kcal fat) or HFD (60% kcal fat) from 6 to 26 weeks of age. Glucose tolerance testing (GTT) was performed at 24 weeks of age, and mice were euthanized at 26 weeks. (*B*) Body mass, body fat, and GTT outcomes across each diet and genotype group (AUC = glucose area under the curve). (*C*) Representative histological images of cartilage structure from the lateral tibial plateau for each diet and genotype group. Open arrow shows representative cartilage lesion observed in WT-HFD animals. Scale bar = 100 μm. (*D*) Representative histological images of osteophyte structure and synovium from the medial tibial plateau for each diet and genotype group. Open arrow heads show osteophyte margins observed in HFD animals. Asterisk shows representative synovial hyperplasia observed in WT-HFD animals. Scale bar = 100 μm. (*E*) Semi-quantitative OA pathology grading outcomes. The OARSI score represents cartilage pathology (0–6 score range), averaged for four joint sites (medial/lateral, femur/tibia) in all sections. The osteophyte score (0–3 range) was evaluated for the medial tibia, averaged for all sections. The synovitis score (0–1 range) shows the average for medial and lateral compartments from all sections. Individual animal data (male mice only) are shown as closed circles. Boxes represent the 25th to 75th percentiles, the horizontal line indicates the median, and whiskers demonstrate maximum and minimum values. Two-way ANOVA p values provided in Table S2. Post hoc paired comparisons ($p < .10$) shown.

(log2_Fc threshold of 0.6) and ($p < .05$). Gene ontology enrichment analysis was based on cluster-specific genes that were seen in at least 25% of the cells in the cluster and that showed at least a 1.5-fold change with FDR-corrected statistical difference of qFDR < 0.05. Enrichment analyses were limited to qFDR < 0.05 and prioritized based on a composite score combining qFDR and fold-enrichment values. PCA analysis were performed using an online tool (https://scienceinside.shinyapps.io/mvda/) built in an R environment. Chondrogenic pellet projected cross-sectional area was analyzed by one-way ANOVA (culture medium treatments) or two-way ANOVA (culture medium treatments and genotype), with Tukey's HSD post hoc analysis ($p < .05$). Statistical tests utilized Prism 9.3.1 (GraphPad Software) and JMP Pro 16.0.0 (SAS Institute).

Results

Cartilage *Sirt3* depletion prevented HFD-induced cartilage pathology and synovitis

To test whether *Sirt3* deletion in cartilage would increase OA pathology caused by feeding mice a HFD, we administered tamoxifen to WT and iC-Sirt3 KO mice 1 week before initiating diet treatments from 6–26 weeks of age (Fig. 1*A*). We evaluated the extent of *Sirt3* deletion by performing SIRT3 immunostaining on joint tissues collected at the completion of the study. In male mice, cartilage SIRT3 was significantly reduced, though not fully absent, in iC-Sirt3 KO mice versus WT mice fed a control or HFD (Fig. S1). However, in female mice, HFD treatment reduced cartilage SIRT3 staining such that cartilage SIRT3 was not different between WT and iC-Sirt3 KO female mice fed a HFD (Fig. S1). HFD-treated iC-Sirt3 KO female mice also gained less body mass and body fat compared to WT mice (Fig. S2). Therefore, we focused on results for male mice for the subsequent HFD animal outcomes. HFD treatment substantially increased body mass and body fat to the same amount in WT and iC-Sirt3 KO mice (Fig. 1*B*). Although fasting blood glucose was not elevated by HFD treatment for either genotype, glucose tolerance was similarly worsened by a HFD compared to the control diet for WT and iC-Sirt3 KO mice (Fig. 1*B*). These results indicate that the *Acan-Cre^{ERT2}* model used for inducible cartilage deletion of *Sirt3* did not markedly alter the systemic metabolic response to HFD treatment in male mice.

Diet-induced obesity significantly increased knee OA pathology in WT mice (Fig. 1*C,D*), as shown by increased cartilage OARSI, osteophyte, and synovitis scores in HFD versus control diet (Fig. 1*E*, Table S2). OA scoring was not different between WT and iC-Sirt3 KO fed a control diet. However, diet-induced obesity did not increase OARSI and synovitis scores in iC-Sirt3 KO mice (Fig. 1*E*), resulting in less cartilage and synovial pathology in iC-Sirt3 KO versus WT mice fed a HFD. *Sirt3* depletion in cartilage did not alter the development of osteophytes under either diet condition.

Cartilage *Sirt3* depletion suppressed HFD-induced changes in cartilage metabolic and inflammatory biomarkers

To further evaluate the effects of *Sirt3* depletion and HFD, we screened cartilage isolated from the knee joints for changes in the expression of genes involved in cartilage extracellular matrix homeostasis, cellular stress, and metabolism (Tables S1 and S2) (Fig. 2*A*). *Sirt3* depletion reduced the expression of *Nox4* and *Acan* (Fig. 2*B*) and increased the expression of *Rela* and *Casp1* (Fig. 2*C*) independently of diet. HFD upregulated the expression of one gene, *Angptl4*, in both WT and iC-Sirt3 KO mice. *Angptl4* is a *Ppar*δ target gene induced by FAs. However, like the cartilage pathology outcome, we observed several genotype-dependent effects of HFD on cartilage gene expression. Notably, HFD upregulated several genes in WT mice only, including *Cfb*, *Epas1*, and *Map1lc3a* (Fig. 2*D*). *Cfb* and *Epas1* are inflammatory mediators previously linked to OA.[22,23]

We next used targeted MS to analyze the protein isolated from the same knee cartilage samples. This analysis revealed numerous diet and genotype-dependent changes in the abundance of proteins regulating metabolism and redox homeostasis (Fig. 3*A*, Table S3). Cluster-based analysis of normalized protein abundance data were grouped and visualized by heatmap. Cluster I proteins were more abundant in iC-Sirt3 KO mice, especially in the control diet condition. Pathway analysis showed these proteins were significantly overrepresented in glycolysis, pentose phosphate, and hypoxia-inducible factor-1 signaling pathways (Fig. 3*B*). Indeed, nearly all glycolysis enzymes were more abundant in the cartilage of iC-Sirt3 KO versus WT under control diet conditions (Fig. 3*C*). Cluster II proteins were more abundant in HFD versus control diet conditions, and these proteins were associated with FA metabolism, branched chain amino acid degeneration, and tryptophan metabolism pathways (Fig. 3*A,B*). However, the magnitude of this difference was less with *Sirt3* depletion for several proteins critical for FA transport and metabolism (e.g., CD36, FABP4, ACAA1, and CPT1A) (Fig. 3*C*). Cluster III proteins were associated with tricarboxylic acid (TCA) cycle, pyruvate metabolism, and glycolysis metabolism pathways and were generally more abundant in iC-Sirt3 KO versus WT, although the difference was less than in cluster I proteins. Few significant differences due to diet or genotype were observed in cluster IV proteins, which were associated with glutathione, TCA cycle, peroxisome, and amino acid metabolism (Fig. 3*A,B*). Overall, cartilage proteomic data suggest that *Sirt3* depletion resulted in a more glycolytic metabolic phenotype that was resistant to HFD-induced shift toward FA metabolism.

Sirt3 deletion reduced chondrocyte oxidative phosphorylation and increased glycolysis

Proteomic data predicted that cartilage *Sirt3* deletion would increase glycolysis and suppress a shift toward FA oxidation in response to HFD. We took two approaches to functionally evaluating the effects of *Sirt3* deletion on chondrocyte metabolism. First, we performed GC–MS metabolic profiling of cartilage harvested from the proximal femoral epiphysis (i.e., hip cap) of 5-week-old WT and *Sirt3 KO* mice. We recently described the advantages of this optimized approach compared to in vitro models for characterizing cartilage metabolism.[19] Principal component (PC) analysis of the relative abundance levels of detected metabolites showed genotype-dependent clustering of samples across PC1, which accounted for approximately 70% of the data variance (Fig. 4*A*). We next compared the relative abundance values of the 12 most influential metabolites contributing to PC1, which were primarily nitrogen-based metabolites and TCA cycle intermediates. This comparison showed that most metabolites were less abundant in cartilage from *Sirt3 KO* mice compared to WT mice (Fig. 4*B*, Table S4).

Next, we compared cellular metabolic rates in primary juvenile chondrocytes isolated from WT and *Sirt3 KO* mice using Seahorse XF assays. Basal proton efflux rate, a measure of glycolysis, was nearly 40% faster in *Sirt3 KO* cells versus WT cells ($p = .038$)

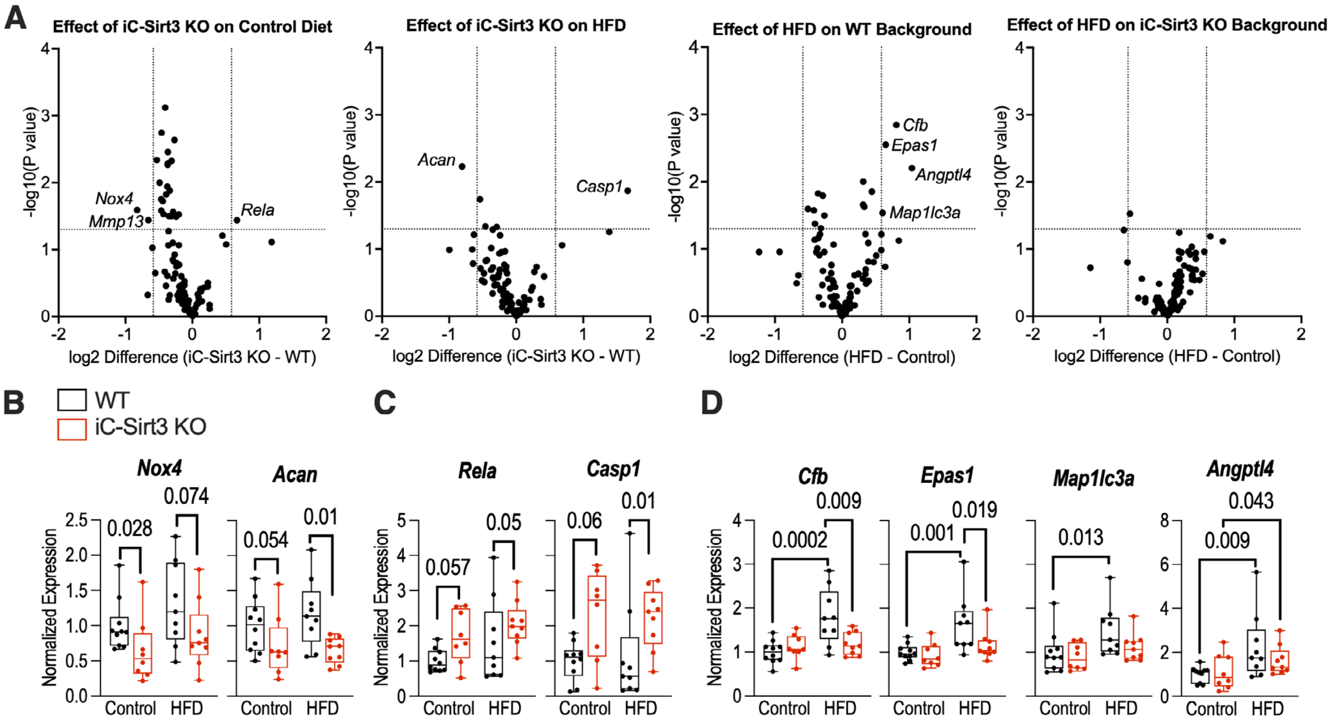

Fig. 2. Inducible cartilage deletion of *Sirt3* (iC-Sirt3 KO) reduced the effect of a HFD on the upregulation of proinflammatory and metabolic genes. Differential gene expression was evaluated for diet- and genotype-dependent effects in cartilage harvested from WT and iC-Sirt3 KO mice fed a control diet or HFD from 6 to 26 weeks of age. Samples were evaluated across a custom-designed panel of 90 genes involved in cartilage extracellular matrix homeostasis, cellular stress, and metabolism (Table S1). (*A*) Genotype and diet effects were evaluated individually using log2 transformed volcano plot comparisons. Labeled genes have a $p < .05$ and log 2-transformed differential expression value ± 0.68 (1.5-fold change). Genes with (*B*) downregulated or (*C*) upregulated expression in cartilage from iC-Sirt3 KO mice compared to WT mice fed a control or HFD. (*D*) HFD-induced changes in cartilage gene expression were primarily observed in WT animals. Gene expression data normalized to the average value of the WT control diet samples for each gene. Two-way ANOVA p values provided in Table S2. Post hoc paired comparisons ($p < .10$) shown.

(Fig. 4*C*,*D*). Conversely, basal oxygen consumption rate, a measure of mitochondrial oxidative phosphorylation, was 25% slower in *Sirt3 KO* cells versus WT cells ($p = .032$) (Fig. 4*E*,*F*). ATP-linked oxygen consumption rate was similarly slower in *Sirt3 KO* cells ($p = .038$), indicating that *Sirt3* deletion reduces mitochondrial energy production in chondrocytes. This reduction in mitochondrial respiration with *Sirt3* deletion does not appear to be due to impaired electron transfer as the rate of proton leak was not elevated in *Sirt3 KO* cells (Fig. 4*E*,*F*). Together, the GC–MS and Seahorse data indicate that *Sirt3* deletion alters chondrocyte metabolism.

Sirt3 deletion increased gene response to hypoxia and IL-1β

To evaluate the potential mechanisms by which *Sirt3* deletion alters chondrocyte function, we measured the expression of genes involved in cartilage extracellular matrix homeostasis and metabolism in primary juvenile chondrocytes isolated from WT and *Sirt3 KO*. We challenged the cells by culturing them under various physiologic stress conditions, including hypoxia, IL-1ß, and FAs. Compared to basal conditions, these stressors altered the expression of most anabolic and catabolic cartilage matrix genes (Fig. 5*A*,*B*). However, *Sirt3* deletion had minimal effect on these transcriptional responses. We instead observed effects of *Sirt3* deletion on the expression of genes regulating growth factors and transcription. *Sirt3* deletion increased *Sox9* expression under hypoxia and *Ppargc1a* under FAs (Fig. 5*C*). Similarly, *Bmp2* and *Tgfbr1* were expressed at greater levels in *Sirt3 KO* cells versus WT with IL-1ß challenge (Fig. 5*C*). Hypoxia inducible factor (HIF)-1a binds to the *Sox9* promoter to regulate *Sox9* expression,[24] and IL-1ß stabilizes HIF-1a in human chondrocytes.[25] We found that *Hif1a* expression was greater in *Sirt3 KO* cells following IL-1ß challenge (Fig. 5*D*). Moreover, hypoxia-responsive genes *Ldha*, *Pfkl*, and *Vegfa* were expressed at greater levels in *Sirt3 KO* cells under both hypoxia and IL-1ß challenge conditions (Fig. 5*D*).

Single-cell RNA sequencing identified *Sirt3*$^+$ chondrocyte population within a heterogeneous primary murine cartilage cell culture model

A common primary cell model used for investigating chondrocyte function in vitro involves isolating cartilage cells from the distal femur and proximal tibia epiphyses of mouse pups 6–8 days after birth. This method, generally referred to as the juvenile murine chondrocyte culture model,[20] utilizes P0 or P1 cells cultured in monolayer and expanded to confluency. We used this model with cells isolated from WT and *Sirt3 KO* mice to generate the data shown in Figs. 4*C*–*F* and 5. However, in preliminary

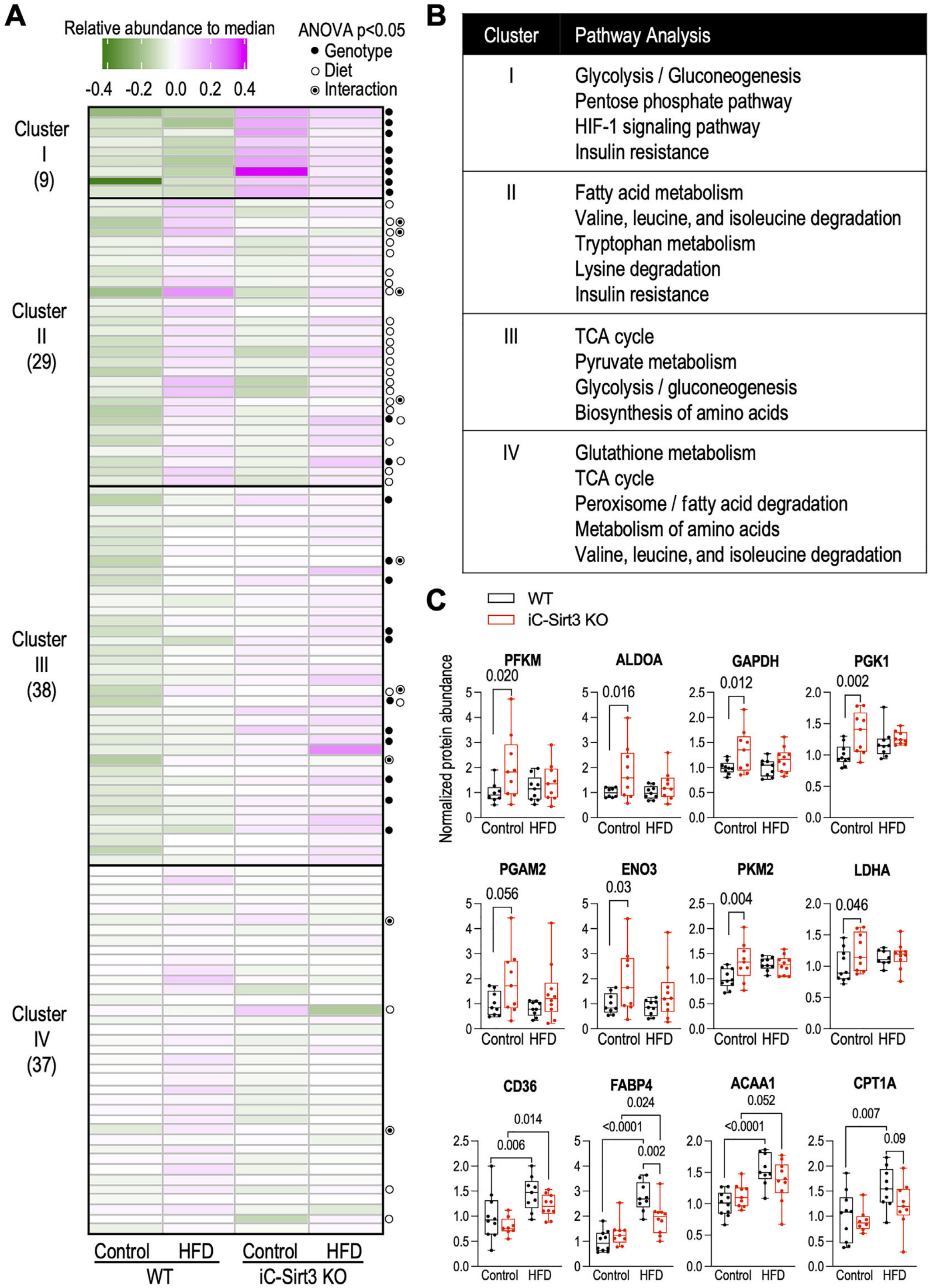

Fig. 3. Inducible cartilage deletion of *Sirt3* (iC-Sirt3 KO) increased glycolytic enzyme protein abundance and suppressed HFD-induced increase in FA metabolism proteins in cartilage. Protein abundance was measured by selected reaction monitoring (SRM) mass spectrometry in cartilage harvested from WT and iC-Sirt3 KO mice fed a control diet or HFD from 6 to 26 weeks of age. The targeted panel included 113 proteins involved in cellular metabolism and redox homeostasis (Table S3). (*A*) Heat map of log-transformed protein abundance values normalized to the median, across all diet and genotype conditions. Proteins were grouped in clusters based on Euclidean distance dissimilarity matrix and partitioning around the medoids algorithm. Cluster number (I–IV) determined by silhouette algorithm. Two-way ANOVA outcomes indicated at right margin for each protein as follows: closed circle ($p < .05$ for genotype), open circle ($p < .05$ for diet), bullseye ($p < .05$ for interaction). (*B*) Top significant predicted pathways (qFDR < 0.05) associated with proteins in each cluster based on pathway analysis performed using STRING database over Kyoto Encyclopedia of Genes and Genomes background. (*C*) Cartilage protein abundance data for WT and iC-Sirt3 KO mice fed a control diet or HFD. Data normalized to average value of WT control diet samples for each protein. Protein abundance and two-way ANOVA p values for all proteins provided in Table S3. Post hoc paired comparisons ($p < .10$) shown.

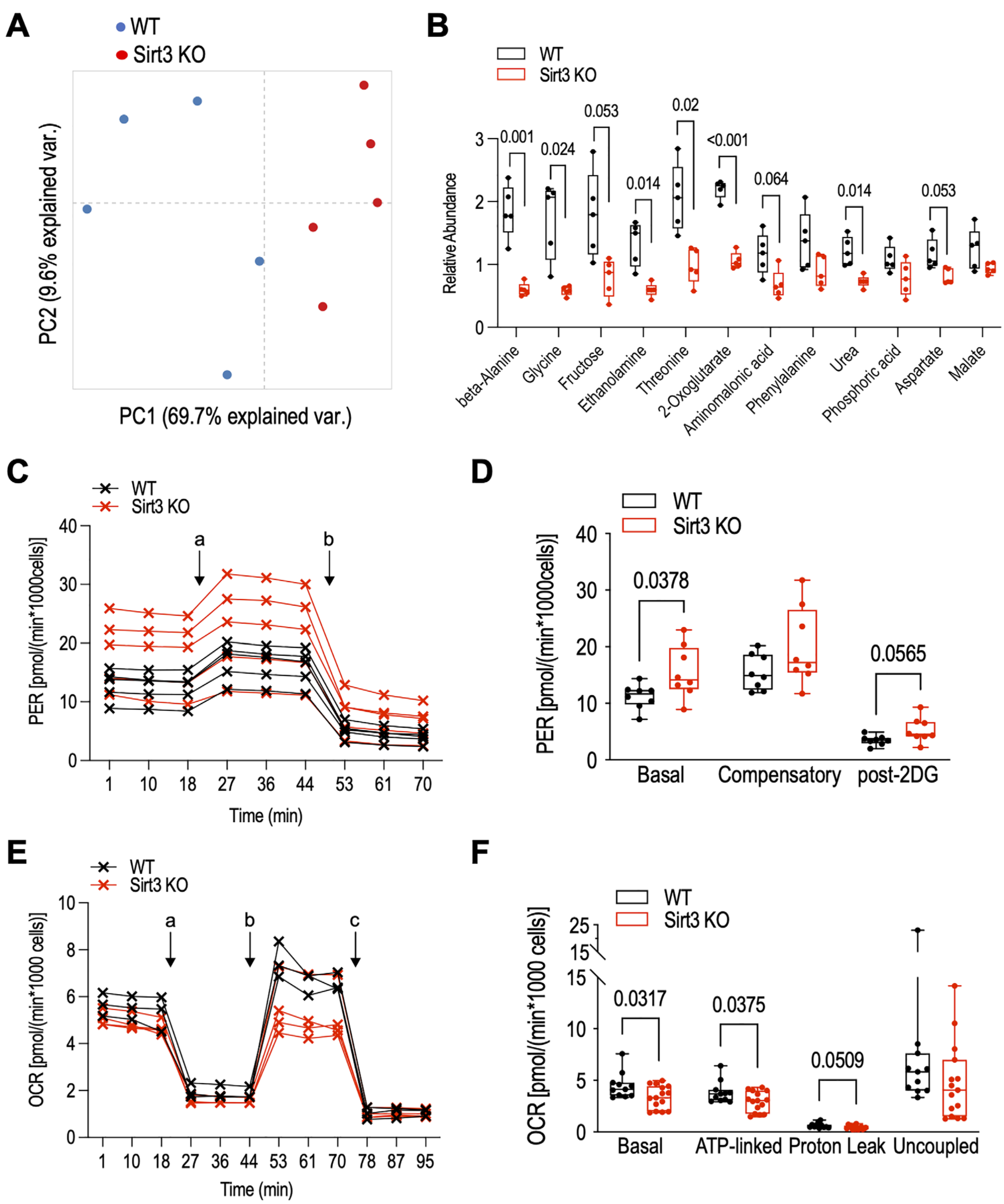

Fig. 4. *Sirt3* deletion altered the abundance of numerous metabolites and promoted a mitochondrial to glycolytic shift in chondrocyte metabolism. (*A*) Principal component (PC) analysis of relative metabolite abundance measured by GC–MS semi-targeted metabolic profiling of femoral head (hip) cartilage from WT (blue) and *Sirt3 KO* (red) 5-week-old mice (Table S4). Each point is an independent biological replicate consisting of cartilage pooled from four animals. (*B*) Relative abundance of the 12 most influential metabolites contributing to the first PC. Post hoc paired comparisons ($p < .10$) shown. (*C*) Representative proton efflux rate (PER) data for seahorse XF glycolytic rate assay comparing primary juvenile chondrocytes isolated from WT (black) and *Sirt3 KO* (red) mice tested on the same plate. Each "x" symbol is the average value of technical duplicates, and lines connect data from the same donor. "a" indicates addition of Rot/AA and "b" addition of 2-DG, as per manufacturer's protocol. (*D*) Summary of glycolytic rate assay results comparing WT and *Sirt3 KO* cells. Each point represents the average of two technical replicates from cells isolated from separate animals. (*E*) Representative oxygen consumption rate (OCR) data for seahorse XF cell Mito stress test assay comparing primary juvenile chondrocytes isolated from WT and *Sirt3 KO* mice tested on same plate. "a" indicates addition of oligomycin, "b" addition of FCCP, and "c" addition of Rot/AA, as per manufacturer's protocol. (F) Summary of Mito stress test assay results comparing WT and *Sirt3 KO* cells. Post hoc paired comparisons ($p < .10$) shown.

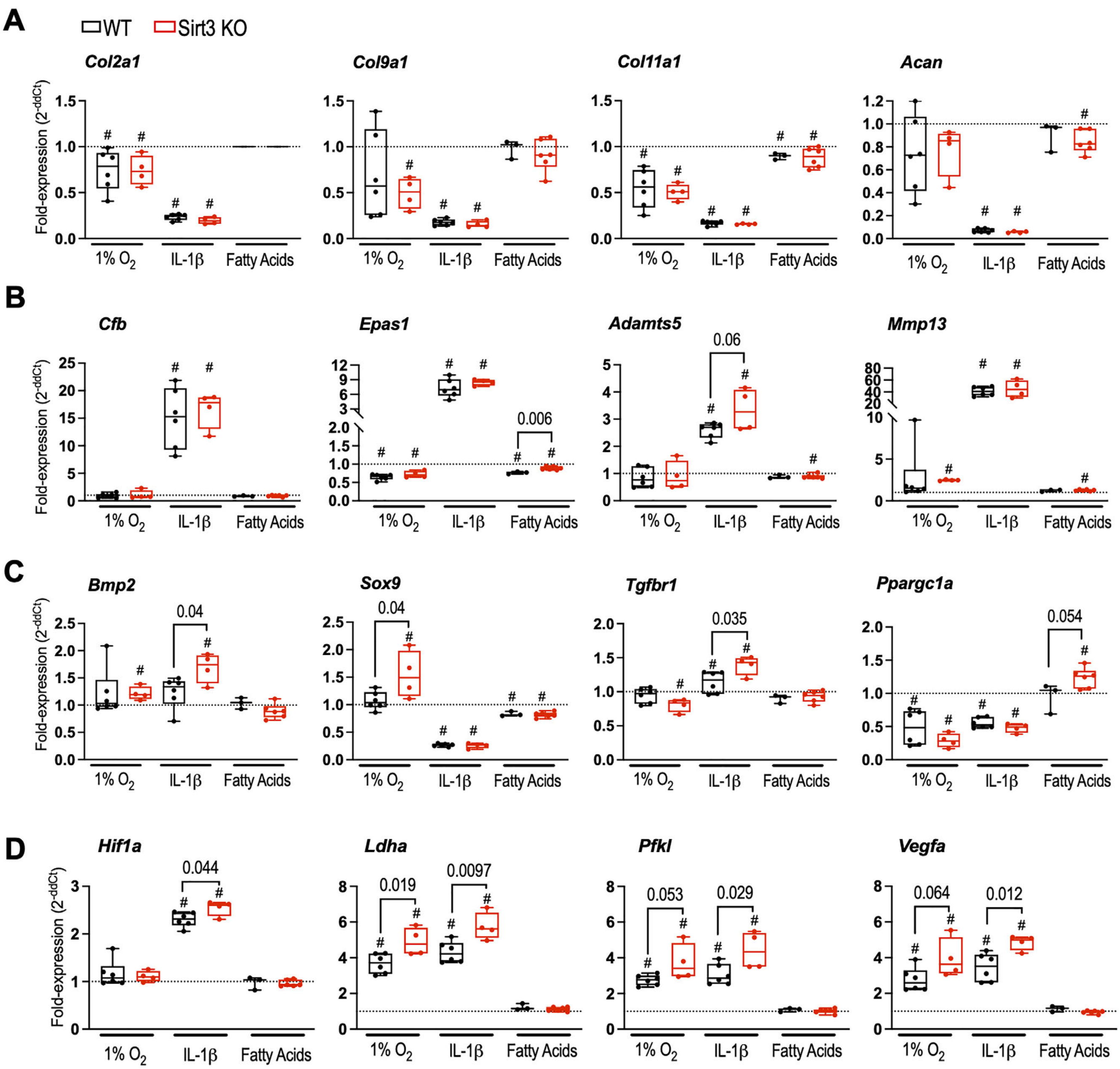

Fig. 5. *Sirt3* deletion increased gene expression response to hypoxic, inflammatory, and FA conditions. Primary juvenile chondrocytes were isolated from the hindlimb epiphyses of postnatal 6- to 8-day-old WT and *Sirt3 KO* mice cultured ±1% hypoxia, 10 ng/mL IL-1β, or 0.5 mM FAs. Data presented as fold-change gene expression normalized to the basal culture condition (dashed line) using the delta–delta Ct method. Results shown for (*A*) cartilage matrix genes, (*B*) proinflammatory and procatabolic genes, (*C*) genes regulating growth factors and transcription, and (*D*) hypoxia response element target genes. Note, *Col2a1* data did not pass quality control standards for the FA culture experiment and are not reported. #$p < .05$ versus genotype-matched basal culture condition. Bars and p values indicate paired comparisons ($p < .10$) between WT and Sirt3 KO cells. Individual cell donor data are shown as closed circles. Boxes represent 25th to 75th percentiles, the horizontal line indicates the median, and whiskers indicate maximum and minimum values.

experiments, we isolated cells from iC-Sirt3 KO mice (i.e., $Sirt3^{fl/fl}Acan\text{-}Cre^{ERT2}$) and were only able to attain a 50% reduction in SIRT3 protein and gene expression after dosing cells with 4-Hydroxytamoxifen (data not shown). These results suggested that only half of the cells may be considered mature chondrocytes. Therefore, we used scRNA-seq to transcriptionally characterize the heterogeneity of WT cartilage cells generated with this model.

Transcriptional heterogeneity was visualized by Uniform Manifold Approximation and Projection (UMAP) analysis, which showed one large contiguous cellular cluster and a small noncontiguous cluster. We next evaluated the distribution of *Col1a1* and *Col2a1* expression, which revealed a roughly equal and nonoverlapping division of cells expressing these genes within the large contiguous group of cells (Fig. 6*A*). Based on the UMAP distributions and division of *Col1a1* and *Col2a1* expressing cells, we

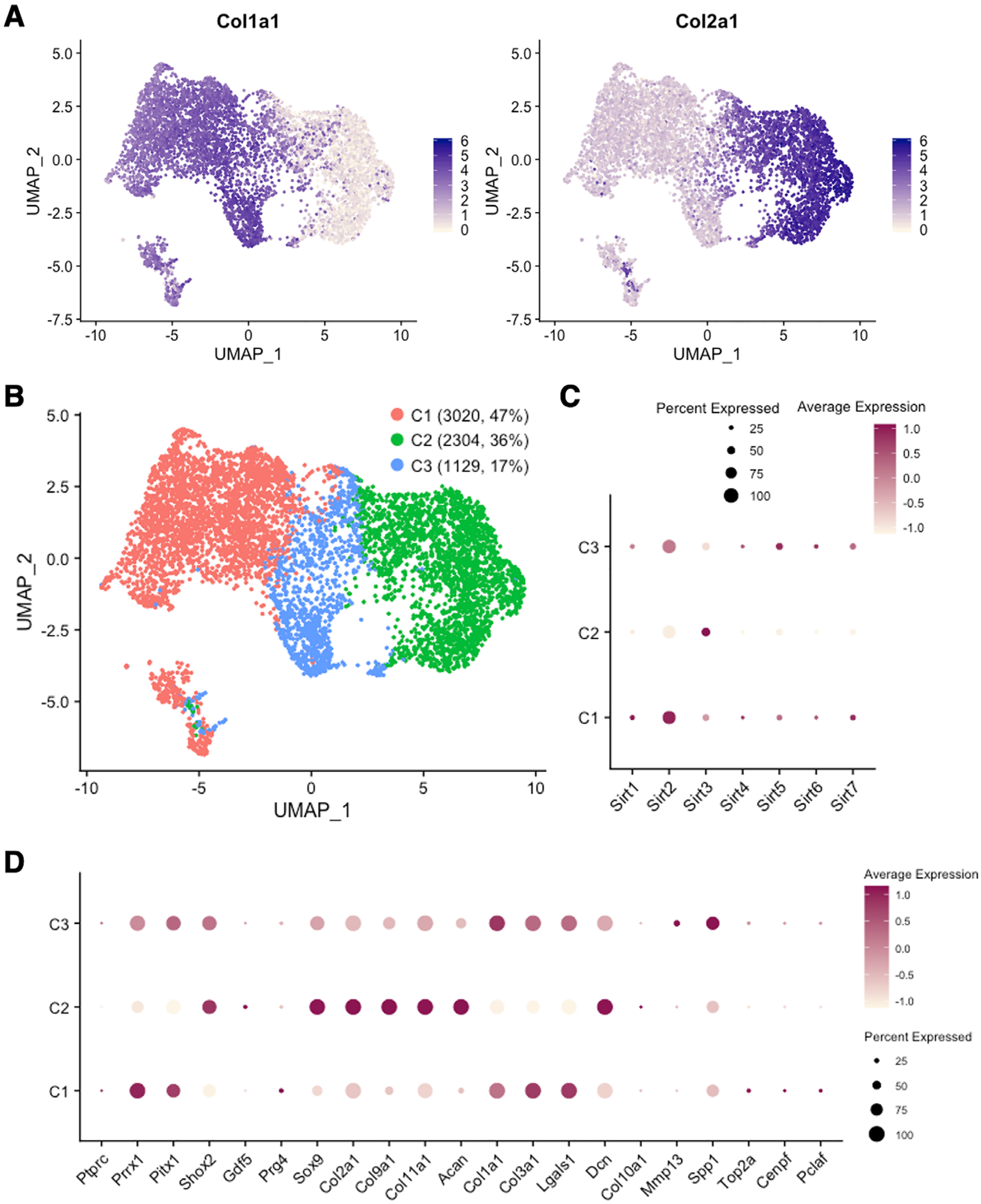

E

Cluster	Top Predicted GO Biological Process Based on Differential Analysis
C1	Extracellular matrix organization
C2	Cartilage development
C3	Ossification

(Figure legend continues on next page.)

set the k.parameters value to [(6453/3) − 1] to refine nearest-neighbor parameters for cluster analysis. This approach generated three clusters, which we defined as C1 (47% total), C2 (36% total), and C3 (17% total) (Fig. 6*B*). We compared the expression patterns of sirtuins 1–7 across each of the three cell clusters (Fig. 6*C*). *Sirt2* showed the most robust expression among all the sirtuins and was greatest in cluster C1, followed by C3. Notably, the only sirtuin that was expressed in cluster C2 was *Sirt3*. Moreover, *Sirt3* expression was negligible in clusters C1 and C3.

To characterize these clusters, we evaluated the expression pattern of select genes based on in vivo studies of limb and joint development, including a study using scRNA-seq.[26] *Ptprc*, the gene encoding the hematopoietic stem cell-derived cell surface protein CD45, was negligibly expressed across all clusters (Fig. 6*D*). Next, we compared *Prrx1*, *Pitx1*, and *Shox2*. These genes are largely expressed by mesenchymal progenitor and chondroprogenitor cells at the early stage of limb development (E12.5).[26] *Prrx1* and *Pitx1* were strongly expressed in C1 and, to a lesser extent, C3. In contrast, *Shox2* was primarily expressed in C2 and, to a lesser extent, C3. Other genetic markers of chondroprogenitor cells, such as *Gdf5* and *Prg4*, were expressed in a small fraction of cells present in C2 and C1, respectively (Fig. 6*D*). Genes associated with mature articular chondrocytes (*Sox9*, *Col2a1*, *Col9a1*, *Col11a1*, and *Acan*) were most strongly expressed in the C2 cluster (Fig. 6*D*). In contrast, genes associated with articular fibrous capsule and meniscus-fated cells (*Col1a1*, *Col3a1*, *Lgals1*, and *Dcn*)[26] were more highly expressed in C1 and C3, except for *Dcn* (Fig. 6*D*). Genes associated with hypertrophic chondrocytes (*Col10a1*, *Mmp13*, and *Spp1*) were most enriched in the C3 cluster. The small noncontiguous population of mostly C1 cells in the lower left quadrant of the UMAP projection (Fig. 6*B*) were identified as actively dividing cells due to cell cycle gene enrichment (*Top2a*, *Cenpf*, and *Pclaf*).

We conducted gene ontology analysis using pairwise cluster-specific differential gene expression (Table S5) to identify enriched biological processes for each cluster (Fig. 6*E*). The C1 cluster was primarily characterized by extracellular matrix organization, with additional processes including collagen fibril organization and mesenchymal cell proliferation. Cluster C2 was primarily characterized by chondrocyte differentiation and cartilage development processes. Finally, C3 was enriched for ossification-related genes compared to C1 and C2. Thus, gene ontology enrichment analysis indicates that the primary monolayer culture model of juvenile chondrocytes contains cells related to mesenchymal progenitor cell function and extracellular matrix organization (cluster C1), cells with clear chondrogenic characteristics (cluster C2), and chondrocyte-like cells with an ossification and mineralization phenotype (cluster C3). Notably, this cellular heterogeneity also appears to extend to metabolic heterogeneity based on the cluster-specific expression patterns of genes involved in the central metabolic pathways of glycolysis, the TCA cycle, FA oxidation, and amino acid catabolism (Fig. S4).

Sirt3 deletion reduces expression of ER-associated degradation pathway genes in mature chondrocytes

To characterize the effect of *Sirt3* deletion specifically in mature chondrocytes, we conducted a second set of scRNA-seq experiments to compare WT and *Sirt3 KO* cells. Cryopreserved passage 1 cells were used for these experiments so that genotype- and sex-specific donor cells isolated from three separate litters could be labeled with unique oligo hashtags and simultaneously loaded in the 10× Chromium Controller. UMAP visualization of transcriptional heterogeneity showed one large contiguous cellular cluster (clusters A [50% total] and B [33% total]) and a moderate noncontiguous cluster defined as cluster C [17% total] (Fig. 7*A*). Cluster A gene expression patterns align with mature chondrocyte genes, like cluster 2 in the prior analysis (Fig. 7*B*). Conversely, cluster B gene expression patters correspond to genes associated with articular fibrous capsule and meniscus-fated cells (Fig. 7*B*). However, unlike the prior experiment using P0 cells, the third cluster in this experiment (cluster C) corresponds to a relatively larger proportion of actively dividing cells (Fig. 7*B*).

Cells isolated from WT and *Sirt3 KO* animals were evenly distributed throughout the UMAP plot and across each cluster (Fig. 7*C,D*). The proportions of cells in each cluster were not different between male and female donors from either genotype (data not shown). We next performed a gene set enrichment analysis (GSEA) based on differentially expressed genes between all *Sirt3 KO* and WT cells. Gene Ontology (GO) sets with the highest enrichment scores were associated with the extracellular matrix and collagen metabolic processes, whereas the GO sets with the lowest enrichment were associated with endoplasmic reticulum (ER) stress and the ER-associated degradation (ERAD) pathway (Fig. 7*E*). We next focused on *Sirt3*-dependent effects specifically in mature chondrocytes by performing a volcano plot analysis of differentially expressed genes between *Sirt3 KO* and WT cells only from cluster A (Fig. 7*F*). *Sirt3* deletion increased the expression of 19 genes and decreased the expression of 16 genes compared to WT cells. To understand the potential functional relevance of these differentially expressed genes, we performed a GO enrichment analysis. This analysis indicates that the loss of *Sirt3* in mature chondrocytes alters genes associated with ER stress, the ERAD pathway, and collagen-containing extracellular matrix (Fig. 7*G*). Notably, ERAD pathway activity is necessary for cartilage development, and disruption of genes in this pathway impairs chondrogenesis.[28]

(Figure legend continued from previous page.)

Fig. 6. Single-cell RNA sequencing revealed a *Sirt3*$^+$ chondrocyte population within a heterogeneous primary cartilage cell model. P0 primary juvenile murine chondrocytes were isolated from WT mice and expanded in monolayer for 4 days in vitro prior to single-cell barcoding and sequencing. 7945 cells were captured for sequencing with a median unique molecular identifier (UMI) count of 25,544 per cell and a median of 4703 genes detected per cell. Based on technical and biological parameters, we excluded from further analysis cells with <1.5% or >5% of UMI counts attributed to mitochondrial genes and <2500 or >7500 total detected genes, resulting in a final analysis of 6453 cells (Fig. S3). (*A*) UMAP projection of 6453 cells based on transcripts of the top 2000 most variably expressed genes. *Col1a1* and *Col2a1* expression was nearly equal and nonoverlapping. (*B*) K-nearest neighbor and Louvain clustering algorithm generated three cellular subclusters, defined as C1, C2, and C3. Figure legend includes cluster-specific total cell number and percent total. (*C*) Cluster-specific expression of sirtuin genes (*Sirt1–7*). (*D*) Cluster-specific expression of genes includes markers of hematopoietic stem cell–derived cell populations (*Ptprc*), limb and joint development (*Prrx1* through *Spp1*), and the cell cycle (*Top2a*, *Cenpf*, and *Pclaf*). Dot size corresponds to percentage of cells in which the gene is detected in the cluster. Color of dot indicates mean expression, including cells in which expression was not detected. (*E*) Top enriched biological process based on gene ontology analysis of pairwise differential gene expression comparisons between each subcluster (Table S5).

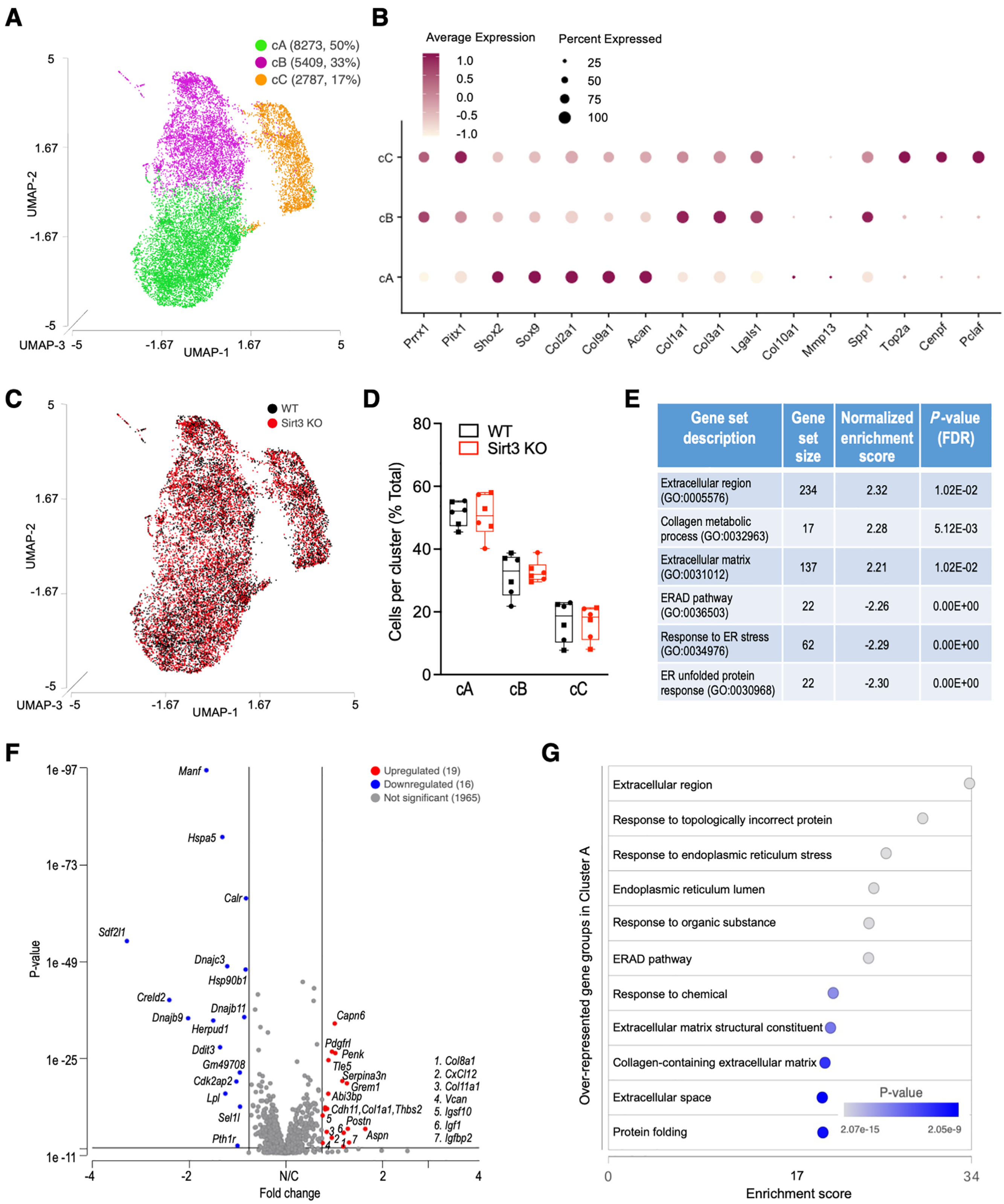

(Figure legend continues on next page.)

Sirt3 deletion impairs BMSC model of chondrogenesis with minimal effect of exogenous FAs

To further investigate the effect of *Sirt3* deficiency on chondrogenesis, we utilized an in vitro BMSC model of chondrogenic pellet growth.[27] Pellets matured into cartilaginous spheroids over the course of 28 days (Fig. S6). We characterized the features of chondrocyte maturation by immunostaining for the mature chondrocyte marker COL2 and the chondrocyte progenitor cell marker PRG4 between 3 and 28 days of culture (Fig. S7). We then compared these spatiotemporal patterns to SIRT3 staining (Fig. S8). SIRT3 was detected throughout the pellet at Day 10. The intensity of SIRT3 staining increased from the center to the edge, like PRG4 at this timepoint. However, by Day 28, SIRT3 staining was restricted to the central two-thirds of the pellet. This staining pattern, which was like that observed for COL2 at this timepoint, resulted in minimal overlap with PRG4. Thus, as with the scRNA-seq data showing that *Sirt3* expression mainly occurred in primary chondrocytes expressing *Col2a1*, the BMSC pellet model of chondrogenesis also showed spatiotemporal alignment of SIRT3 and COL2 staining.

Based on our in vivo findings showing a HFD-dependent effect of *Sirt3* deletion on cartilage degradation, we tested for an interaction of *Sirt3* deletion and elevated FA on chondrogenesis. We first tested whether exogenous FA altered chondrogenesis using WT BMSCs. Between Days 7 and 14 of culture, the medium for two pellets from each donor was supplemented with 500 μM FA or BSA vehicle, and a third pellet was kept in the control culture medium (Fig. 8*A,B*). All pellets were returned to the control culture medium between Day 14 and Day 21. The 7- to 14-day treatment period was selected because this was a time when COL2 production substantially increased, and the pellets developed distinct inner and outer zones. We confirmed that FA treatment increased lipid droplet formation in the pellets as shown by increased perilipin staining (Fig. 8*A*). However, FA treatment did not alter pellet size or safranin-O staining intensity (Fig. 8*A,C*). Pellets subjected to FA and BSA treatments also showed similar growth and safranin-O staining compared to the control pellets (Fig. 8*A,C*).

To test for an interaction between elevated FA and *Sirt3* deletion on chondrogenesis, FA and BSA vehicle treatments were applied to BMSCs harvested from WT and *Sirt3 KO* mice from Day 7 to 14 (Fig. 8*D*). However, unlike the prior experiment, pellets were collected at Day 14 to verify that an acute effect of FA treatment was not missed in the first experiment. The results confirmed that neither FA nor BSA vehicle treatment altered pellet sizes, even when collected immediately after treatment (Fig. 8*D,E*). Overall, cartilage pellets generated from *Sirt3 KO* BMSCs were smaller than WT-derived pellets under all culture conditions (genotype effect, $p = .0448$; Fig. 8*E*). The genotype effect was greatest in the FA treatment condition ($p = .0002$) (Fig. 8*E*). Pellets generated from *Sirt3 KO* BMSCs were also fragmented compared to WT pellets. Based on these changes in cartilage pellet size and integrity, we evaluated the distribution of PRG4 positive cells as a marker of chondroprogenitor cells. In WT pellets, the intensity of PRG4 positive staining increased from the center to the outer edge, forming a ringlike staining pattern along the surface (Fig. 8*D,F*). However, in *Sirt3 KO* pellets, PRG4 positive staining remained distributed throughout the pellets and a surface layer of PRG4 positive cells was absent. FA treatment did not alter the pattern of PRG4 staining in either WT or *Sirt3 KO* pellets (Fig. 8*F*).

Discussion

Our study on the loss of the mitochondrial deacetylase enzyme *Sirt3* in BMSCs, immature cartilage chondrocytes, and mature cartilage provides new evidence linking chondrocyte metabolic regulation and cartilage homeostasis during development and in adulthood. We hypothesized that the combination of HFD-induced obesity and loss of cartilage *Sirt3* at a young age would impair chondrocyte mitochondrial function, leading to cellular stress and accelerated OA pathology. Instead, we unexpectedly found that depletion cartilage *Sirt3* at 5 weeks of age using *Acan*-Cre^{ERT2} mice protected against the development of cartilage degeneration and synovial hyperplasia following 20 weeks of HFD. Negligible differences in joint structure were observed between WT and cartilage *Sirt3*-depleted mice fed a control diet. The protection against HFD-induced changes was associated with greater levels of cartilage glycolytic enzyme proteins compared to WT mice. Furthermore, the HFD-induced upregulation of FA transport and metabolism proteins observed in WT mice was suppressed with cartilage *Sirt3* depletion. Consistent with these findings, *Sirt3* deletion increased the rate of glycolysis and reduced the rate of oxidative phosphorylation in primary juvenile murine chondrocytes. In a developmental context, *Sirt3* deletion reduced cartilage growth using a BMSC cell pellet model of chondrogenesis, and the loss of *Sirt3* reduced the expression of ERAD pathway genes in chondrocytes. Sim and colleagues recently reported that ERAD pathway activity was

(Figure legend continued from previous page.)

Fig. 7. *Sirt3* deletion reduces expression of ER-associated degradation pathway genes in mature chondrocytes. Cryopreserved passage 1 (P1) primary murine juvenile chondrocytes were isolated from WT and *Sirt3 KO* mice and prepared for single-cell RNA sequencing. (*A*) UMAP projection of 16,469 cells based on transcripts of the top 2000 most variably expressed genes. Graph-based clustering using Louvain clustering algorithm generated three cellular subclusters, defined as cA, cB, and cC. Figure legend includes cluster-specific cell number and percent total. (*B*) Cluster-specific expression of genes includes markers of limb and joint development (*Prrx1* through *Spp1*), and the cell cycle (*Top2a*, *Cenpf*, and *Pclaf*). Dot size corresponds to percentage of cells in which the gene is detected in the cluster. Color of dot indicates mean expression, including cells in which expression was not detected. (*C*) UMAP projection of 16,469 cells colored by genotype (WT: black; *Sirt3 KO*: red). (*D*) WT and *Sirt3 KO* cells categorized by cluster and expressed as a percentage of total cells for each donor. Data from individual donor animals shown as closed circles. Boxes represent 25th to 75th percentiles, the horizontal line indicates median, and whiskers indicate maximum and minimum values. Each symbol represents a male or female donor from three separate litters per genotype. (*E*) Gene set enrichment analysis (GSEA) showing gene ontology (GO) gene sets with the three highest and three lowest enrichment scores for differentially expressed genes between *Sirt3 KO* and WT cells. (*F*) Volcano plot of 35 differentially expressed genes (*Sirt3 KO* versus WT) specific to cA cells. Upregulated (red) and downregulated (blue) genes are identified ($p < .05$ and fold-change >1.3). (*G*) GSEA enrichment score plot of gene groups overrepresented in cA cells based on *Sirt3 KO* versus WT differential gene expression analysis.

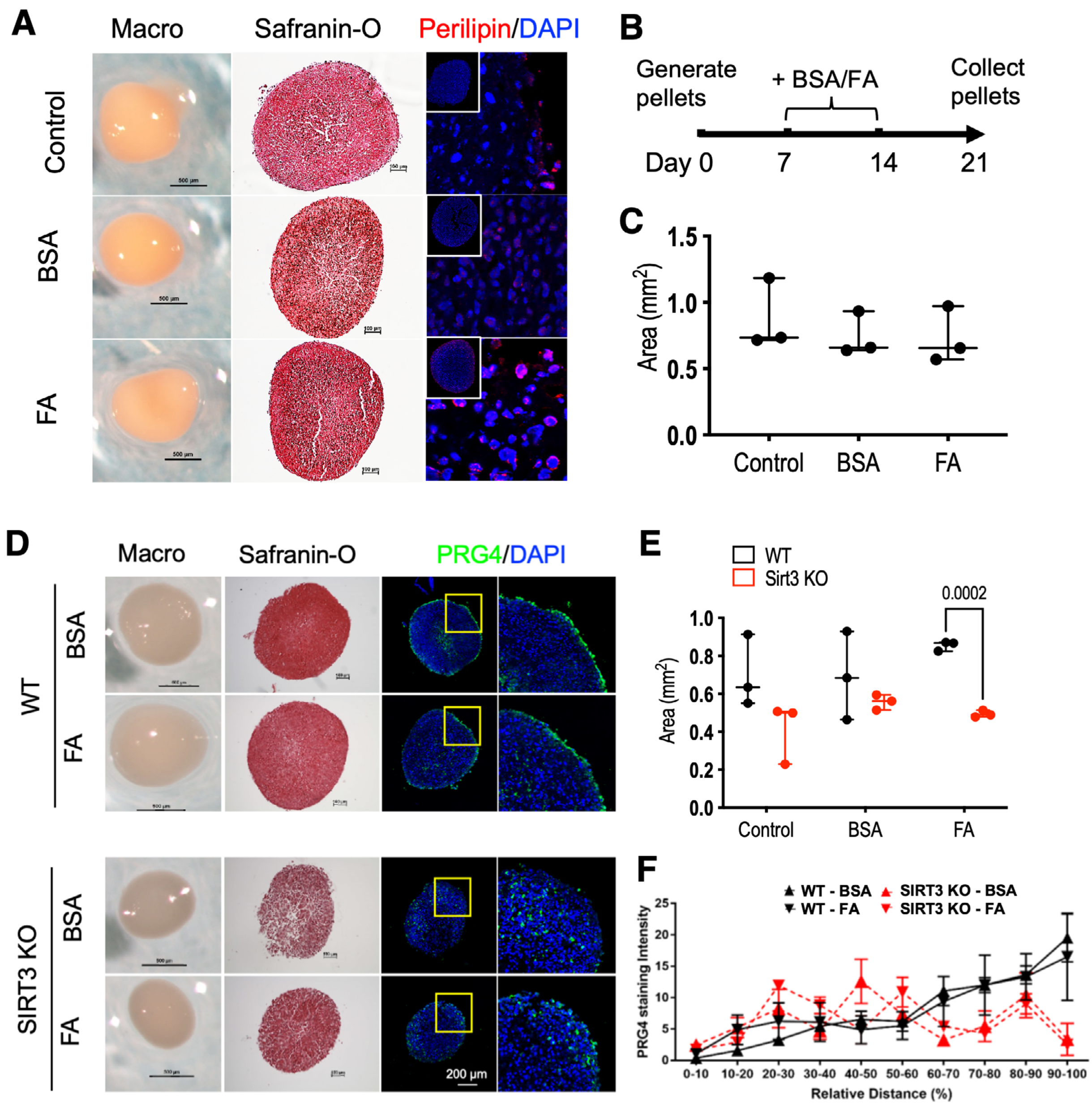

Fig. 8. *Sirt3* deletion impairs chondrogenesis in a bone marrow stem/stromal cell (BMSC) pellet model with minimal effect of exogenous FAs. Cell pellets were cultured in chondrogenic differentiation medium ±1% BSA control or 500 μM FA for up to 21 days. (*A*) Representative macroscopic image pellets (first panel, scale bar = 500 μm), safranin-O staining of histological section (middle panel, scale bar = 100 μm), and immunofluorescent staining for lipid droplet membrane protein, perilipin (third panel). Note the increase in perilipin staining in the FA-treated sample. (*B*) Treatment timeline. Between Days 7 and 14 of culture, two pellets from each donor were supplemented with either 500 μM FA or 1% BSA vehicle, and a third pellet was kept in the control culture media. All pellets were then returned to control media from day 14 to 21. (*C*) Quantification of projected two-dimensional (2D) pellet area calculated from macroscopic image, as shown in panel A. Values = mean ± SD. (*D*) 3D chondrogenic pellets from WT or *SIRT3 KO* donor BMSCs treated with 1% BSA vehicle or 500 μM FA. Macroscopic image (first panel, scale bar = 500 μm), safranin-O staining (middle panel, scale bar = 100 μm), and immunofluorescent staining for PRG4 (third panel, yellow square indicates magnified region shown in image to right.). (*E*) Quantification of projected 2D pellet area calculated from macroscopic images shown in panel D. Values = mean ± SD. (*F*) Quantification of PRG4 fluorescence intensity from center (0%) to edge (100%) of pellet for each treatment. PRG4 staining was reduced in outer edge of *SIRT3 KO* pellets, especially at pellet surface (see panel D). Values = mean ± SEM.

necessary for cartilage development, and disruption of genes in this pathway impaired chondrogenesis.[28] Despite these observations, compensatory mechanisms likely exist to overcome the impact of *Sirt3* deletion on skeletal development as *Sirt3 KO* mice are indistinguishable from young adult (<6-month-old) WT littermates in terms of body mass, long-bone length, and cortical and trabecular bone mass at the femur and spine.[29] In contrast, the loss of *Sirt3* from cartilage during early adulthood resulted in sustained differences in cartilage metabolic enzymes up to 26 weeks of age, which we showed are associated with protection against the development of HFD-induced OA.

The most important finding of this study is that *Sirt3* depletion in cartilage protects, rather than aggravates, HFD-induced OA. This is important because previous evidence supported only a chondroprotective role for *Sirt3*. Prior research showed that *Sirt3* limited oxidative stress, improved mitochondrial DNA integrity, and supported mitochondrial function in chondrocytes.[16,17,30] Furthermore, one of the primary deacetylation targets of *Sirt3* is the mitochondrial antioxidant enzyme *Sod2*, whose function is impaired in age-associated and post-traumatic models of OA. However, as we recently reviewed, few studies have evaluated the contribution of these or other cellular metabolic and redox regulatory mechanisms in obesity-associated models of OA, especially those that exclude joint trauma.[6]

Our data suggest that the initiating mechanism of HFD-induced OA may be distinct from aging and trauma-related processes. For example, we observed minimal changes in redox-associated transcripts and proteins. Rather, HFD significantly altered cellular metabolism pathways in cartilage by upregulating FA transport and metabolism proteins, consistent with our prior findings.[8] Lipid and cholesterol metabolism had been previously tied to cartilage degeneration through the nuclear receptors peroxisome proliferator-activated receptor δ and retinoic acid-related orphan receptor alpha, respectively.[2,31,32] *Sirt3* is a positive regulator of FA oxidation.[13] Thus, one potential explanation for protection resulting from the depletion of *Sirt3* in cartilage is that it suppresses HFD-induced intracellular lipid transport and associated metabolic signaling.

An additional metabolic consequence of *Sirt3* depletion was the upregulation of glycolysis and glycolytic enzyme abundance. Chondrocytes are well characterized for utilizing glycolysis to produce most cellular ATP,[3] and our scRNAseq analysis of primary juvenile murine chondrocytes showed that glycolytic enzymes were most highly expressed in mature chondrocytes compared to other osteochondral progenitor cells. HIF-1a signaling promotes glycolysis, and the loss of *Sirt3* was previously reported to stabilize HIF-1a in breast cancer cells.[33] Our analysis of the expression of HIF-1a target genes under hypoxic and inflammatory conditions was consistent with increased HIF-1a signaling in *Sirt3* deficient chondrocytes. We recognize, however, that enhanced glycolysis is not always chondroprotective. Arra and colleagues recently reported that an inflammation-induced metabolic shift toward glycolysis promoted the production of reactive oxygen species and cartilage catabolism.[34] Thus, our findings suggest it is prudent to consider the molecular mechanisms and physiological context when evaluating whether a particular metabolic phenotype is chondroprotective or damaging.

An intriguing finding from our scRNA-seq profiling analyses was the diversity of cell types within the standard juvenile murine chondrocyte culture model.[20] We were surprised that only 36%–50% of the cells in this model expressed mature chondrocyte genes, whereas other cells expressed genetic markers of limb mesenchymal progenitor cells, chondroprogenitor cells, and osteochondral cells. Despite the limitations of this in vitro culture model, our results support several relevant conclusions. First, among the sirtuins, only *Sirt3* was primarily expressed within the mature chondrocyte population. This supports our focus on *Sirt3* in mature chondrocytes, and it suggests that *Sirt3* functions more in differentiated chondrocytes than chondroprogenitor cells. Second, the similarity in cell cluster proportions between cartilage cells isolated from WT and *Sirt3 KO* mice suggests that *Sirt3* does not modify the differentiation potential of progenitor cells to become mature chondrocytes in the developing joint. However, this does not rule out the potential for *Sirt3* to modify progenitor cell viability, differentiation capacity, or migration within adult cartilage. Our in vitro screening experiments involving hypoxia, IL-1ß, and FA challenges did not reveal any obvious effects of *Sirt3* loss on the expression of catabolic gene networks, although these assays were not specific to the mature chondrocyte population. Future research on how *Sirt3* modifies cartilage regenerative capacity and chondrocyte-specific catabolic processes, including apoptosis and senescence, may uncover additional *Sirt3*-dependent processes relevant to OA pathogenesis.

Our findings reinforce a cell-specific and age-dependent role for *Sirt3* in skeletal homeostasis. In vitro studies of isolated BMSCs and primary murine calvarial osteoblasts indicate a positive role for *Sirt3* in osteoblast differentiation and bone growth.[35,36] We observed *Sirt3*-dependent chondrogenesis in BMSC pellets and ERAD pathway gene expression in mature chondrocytes, indicating a positive role for *Sirt3* in cartilage development. The relevance of these findings to in vivo conditions remains to be determined. Furthermore, although the loss of cartilage *Sirt3* is chondroprotective under HFD conditions at a young age, *Sirt3 KO* mice develop greater OA with age.[16] The age-dependent effects of *Sirt3* are also seen in the skeleton, with 16-month-old *Sirt3 KO* mice exhibiting protection against age-associated loss of bone mass compared to WT littermates.[29] This protection appears to be due to reduced osteoclast resorptive activity linked to impaired mitochondrial function in the absence of *Sirt3*.[29,37] Consistent with these findings, mice that overexpress *Sirt3* show an age-associated increase in bone loss and osteoclastogenesis.[38] Thus, *Sirt3* appears to function in a highly context-dependent manner in the skeleton.

There are several limitations to consider with this study. Foremost, the direct translation of this work to human cartilage has not been established. However, we note that prior studies reported an age-dependent loss of SIRT3 in human cartilage,[16,17] and our findings on *Sirt3*-dependent mitochondrial respiration in mouse chondrocytes replicate a previous report using human chondrocytes.[17] Another limitation is the absence of a direct assessment of *Sirt3*-dependent chondrocyte FA oxidation. Unfortunately, mouse cartilage is too small for a direct assessment, and our scRNAseq analyses show that mature chondrocytes are not the major population of cells expressing FA oxidation enzymes in the primary juvenile monolayer chondrocyte model used for in vitro metabolic testing (Fig. S3). An additional limitation of the primary juvenile chondrocyte model is the use of monolayer culture under atmospheric oxygen, which is a clear departure from in vivo conditions. Our previous research showed that in vitro culture favored amino acid metabolism compared to in vivo conditions.[19] Future studies using different metabolic substrates[39] and culture conditions, such as three-dimensional culture matrix and physiologic oxygen tension, may allow investigators to optimize conditions to generate a more uniform cellular phenotype in this primary murine chondrocyte model. Despite these limitations, we showed that this in vitro culture model retained numerous genetic markers of heterogeneous cell populations that are present in vivo during murine joint development.

In conclusion, a significant challenge in the field is to understand how metabolic stressors, such as those associated with obesity, promote synovial joint tissue damage and impaired function. One reason for this challenge is the complexity of how metabolism contributes to the development, maintenance, and repair of joint tissues. Identifying obesity-dependent metabolic processes that harm cartilage maintenance and repair could create new strategies to prevent or treat OA. Our study represents a significant advance by identifying *Sirt3* as a critical effector gene in chondrocytes under conditions of diet-induced obesity. Based on loss-of-function studies, our findings indicate that *Sirt3* inhibits glycolysis, stimulates mitochondrial respiration and FA metabolism, and promotes the development of HFD-induced OA. These effects appear to be separate from a beneficial role of *Sirt3* in chondrogenesis. Future work is needed to determine whether *Sirt3*-dependent metabolic effects induced by a HFD can be blocked using alternative strategies to protect against the development of obesity-associated OA.

Financial support

This study was supported by the National Institutes of Health (R01AG049058, P30GM114731, P20GM139763), the Oklahoma Center for Adult Stem Cell Research (OCASCR, a program of TSET), the Oklahoma Center for the Advancement of Science and Technology (HF18-022), and the OMRF Clinical Genomics Core. The content is solely the responsibility of the authors and does not necessarily represent the official views of the funding sources, which played no role in the conduct, writing, or submission of the manuscript for publication.

Authors' roles

Shouan Zhu: *conceptualization*, *methodology*, *formal analysis*, *investigation*, *writing—original draft*, *writing—review and editing*, *visualization*, *supervision*, *project administration*.

Elise Donovan: *conceptualization*, *methodology*, *investigation*, *writing—review and editing*, *supervision*, *project administration*.

Dawid Makosa: *formal analysis*, *investigation*, *software*, *writing—review and editing*.

Padmaja Mehta-D'souza: *software*, *validation*, *formal analysis*, *data curation*, *writing—original draft*, *writing—review and editing*, *visualization*, *supervision*, *project administration*.

Anita Jopkiewicz: *methodology*, *formal analysis*, *investigation*, *writing—review and editing*.

Albert Batushansky: *formal analysis*, *software*, *data curation*, *writing—review and editing*, *visualization*.

Dominic Cortassa: *formal analysis*, *writing—review and editing*.

Aaron Simmons: *methodology*, *investigation*, *writing—review and editing*.

Erika Barboza Prado Lopes: *formal analysis*, *validation*, *investigation*, *writing—review and editing*, *project administration*.

Mike Kinter: *methodology*, *formal analysis*, *investigation*, *writing—review and editing*.

Timothy M. Griffin: *conceptualization*, *formal analysis*, *investigation*, *writing—original draft*, *writing—review and editing*, *visualization*, *supervision*, *project administration*, *funding acquisition*. All authors read and approved the final version of the article.

Conflict of interest

The authors have no conflicts of interest to declare.

Acknowledgments

We thank the OMRF Flow Cytometry Core for technical assistance and advice, Rahul Rajala for helpful insight with scRNAseq data analysis, and Drs. Graham Wiley, Joel Guthridge, and Miles Smith for technical assistance and advice with scRNAseq data analysis. Dr. Eric Verdin kindly provided the Sirt3-floxed mice used in this study. Graphical abstract created with BioRender.com.

Author Contributions

Shouan Zhu: Conceptualization; formal analysis; investigation; methodology; project administration; supervision; visualization; writing – original draft; writing – review and editing. **Elise L Donovan:** Conceptualization; investigation; methodology; project administration; supervision; writing – review and editing. **Dawid Makosa:** Formal analysis; investigation; software; writing – review and editing. **Padmaja Mehta-D'souza:** Data curation; formal analysis; project administration; software; supervision; validation; visualization; writing – original draft; writing – review and editing. **Anita Jopkiewicz:** Formal analysis; investigation; methodology; writing – review and editing. **Albert Batushansky:** Data curation; formal analysis; software; visualization; writing – review and editing. **Dominic Cortassa:** Formal analysis; writing – review and editing. **Aaron Simmons:** Investigation; methodology; writing – review and editing. **Erika Barboza Prado Lopes:** Formal analysis; investigation; project administration; validation; writing – review and editing. **Mike Kinter:** Formal analysis; investigation; methodology; writing – review and editing. **Timothy Griffin:** Conceptualization; formal analysis; funding acquisition; project administration; supervision; visualization; writing – original draft; writing – review and editing.

Peer Review

The peer review history for this article is available at https://publons.com/publon/10.1002/jbmr.4721.

Data Availability Statement

Single cell RNA sequencing data are available on GEO (GSE192668). Additional data that support the findings of this study are available from the corresponding author upon reasonable request.

References

1. Collins KH, Lenz KL, Pollitt EN, et al. Adipose tissue is a critical regulator of osteoarthritis. Proc Natl Acad Sci. 2021;118(1):e2021096118.
2. Choi W-S, Lee G, Song W-H, et al. The CH25H–CYP7B1–RORα axis of cholesterol metabolism regulates osteoarthritis. Nature. 2019;566(7743):254-258.
3. Mobasheri A, Rayman MP, Gualillo O, Sellam J, van der Kraan P, Fearon U. The role of metabolism in the pathogenesis of osteoarthritis. Nat Rev Rheumatol. 2017;13(5):302-311.
4. Liu-Bryan R, Terkeltaub R. Emerging regulators of the inflammatory process in osteoarthritis. Nat Rev Rheumatol. 2014;11(1):35-44.
5. June RK, Liu-Bryan R, Long F, Griffin TM. Emerging role of metabolic signaling in synovial joint remodeling and osteoarthritis. J Orthop Res. 2016;34(12):2048-2058.
6. Batushansky A, Zhu S, Komaravolu RK, South S, Mehta-D'souza P, Griffin TM. Fundamentals of OA. An initiative of osteoarthritis and

cartilage. Obesity and metabolic factors in OA. Osteoarthr Cartil. 2022;30(4):501-515.

7. Griffin TM, Fermor B, Huebner JL, et al. Diet-induced obesity differentially regulates behavioral, biomechanical, and molecular risk factors for osteoarthritis in mice. Arthritis Res Ther. 2010;12(4):R130.
8. Donovan EL, Lopes EBP, Batushansky A, Kinter M, Griffin TM. Independent effects of dietary fat and sucrose content on chondrocyte metabolism and osteoarthritis pathology in mice. Dis Models Mech. 2018;11(9):dmm034827.
9. Lu B, Driban JB, Xu C, Lapane KL, McAlindon TE, Eaton CB. Dietary fat intake and radiographic progression of knee osteoarthritis: data from the osteoarthritis initiative. Arthritis Care Res. 2017;69(3):368-375.
10. Alvarez-Garcia O, Rogers NH, Smith RG, Lotz MK. Palmitate has proapoptotic and proinflammatory effects on articular cartilage and synergizes with interleukin-1. Arthritis Rheumatol. 2014;66(7):1779-1788.
11. Wu C-L, Jain D, McNeill JN, et al. Dietary fatty acid content regulates wound repair and the pathogenesis of osteoarthritis following joint injury. Ann Rheum Dis. 2015;74(11):2076-2083.
12. Ji Q, Zheng Y, Zhang G, et al. Single-cell RNA-seq analysis reveals the progression of human osteoarthritis. Ann Rheum Dis. 2019; 78(1): 100-110.
13. Hirschey MD, Shimazu T, Goetzman E, et al. SIRT3 regulates mitochondrial fatty-acid oxidation by reversible enzyme deacetylation. Nature. 2010;464(7285):121-125.
14. Hirschey MD, Shimazu T, Jing E, et al. SIRT3 deficiency and mitochondrial protein hyperacetylation accelerate the development of the metabolic syndrome. Mol Cell. 2011;44(2):177-190.
15. Rardin MJ, Newman JC, Held JM, et al. Label-free quantitative proteomics of the lysine acetylome in mitochondria identifies substrates of SIRT3 in metabolic pathways. Proc Natl Acad Sci. 2013;110(16): 6601-6606.
16. Fu Y, Kinter M, Hudson J, et al. Aging promotes Sirtuin 3-dependent cartilage superoxide dismutase 2 acetylation and osteoarthritis. Arthritis Rheumatol. 2016;68(8):1887-1898.
17. Chen L-Y, Wang Y, Terkeltaub R, Liu-Bryan R. Activation of AMPK-SIRT3 signaling is chondroprotective by preserving mitochondrial DNA integrity and function. Osteoarthr Cartil. 2018;26(11):1539-1550.
18. Lombard DB, Alt FW, Cheng H-L, et al. Mammalian Sir2 homolog SIRT3 regulates global mitochondrial lysine acetylation. Mol Cell Biol. 2007;27(24):8807-8814.
19. Batushansky A, Lopes EBP, Zhu S, Humphries KM, Griffin TM. GC-MS method for metabolic profiling of mouse femoral head articular cartilage reveals distinct effects of tissue culture and development. Osteoarthr Cartil. 2019;27(9):1361-1371.
20. Gosset M, Berenbaum F, Thirion S, Jacques C. Primary culture and phenotyping of murine chondrocytes. Nat Protoc. 2008;3(8):1253-1260.
21. Zhu S, Batushansky A, Jopkiewicz A, et al. Sirt5 deficiency causes posttranslational protein malonylation and dysregulated cellular metabolism in chondrocytes under obesity conditions. Cartilage. 2021;11:1947603521993209.
22. Yang S, Kim J, Ryu J-H, et al. Hypoxia-inducible factor-2alpha is a catabolic regulator of osteoarthritic cartilage destruction. Nat Med. 2010;16(6):687-693.
23. Wang Q, Rozelle AL, Lepus CM, et al. Identification of a central role for complement in osteoarthritis. Nat Med. 2011;17(12):1674-1679.
24. Amarilio R, Viukov SV, Sharir A, Eshkar-Oren I, Johnson RS, Zelzer E. HIF1α regulation of Sox9 is necessary to maintain differentiation of hypoxic prechondrogenic cells during early skeletogenesis. Development. 2007;134(21):3917-3928.
25. Murata M, Yudoh K, Nakamura H, et al. Distinct signaling pathways are involved in hypoxia- and IL-1-induced VEGF expression in human articular chondrocytes. J Orthop Res. 2006;24(7):1544-1554.
26. Bian Q, Cheng Y-H, Wilson JP, et al. A single cell transcriptional atlas of early synovial joint development. Development. 2020;147(14): dev185777.
27. Solchaga LA, Penick KJ, Welter JF. Chondrogenic differentiation of bone marrow-derived mesenchymal stem cells: tips and tricks. Methods Mol Biol. 2011;698:253-278.
28. Sim HJ, Cho C, Kim HE, et al. Augmented ERAD (ER-associated degradation) activity in chondrocytes is necessary for cartilage development and maintenance. Sci Adv. 2022;8(3):eabl4222.
29. Ling W, Krager K, Richardson KK, et al. Mitochondrial Sirt3 contributes to the bone loss caused by aging or estrogen deficiency. JCI Insight. 2021;6(10):e146728.
30. Zhu S, Makosa D, Miller B, Griffin TM. Glutathione as a mediator of cartilage oxidative stress resistance and resilience during aging and osteoarthritis. Connect Tissue Res. 2019;15(6):1-14.
31. Ratneswaran A, Sun MM-G, Dupuis H, Sawyez C, Borradaile N, Beier F. Nuclear receptors regulate lipid metabolism and oxidative stress markers in chondrocytes. J Mol Med. 2017;95(4):431-444.
32. Ratneswaran A, LeBlanc EA, Walser E, et al. Peroxisome proliferator-activated receptor δ promotes the progression of posttraumatic osteoarthritis in a mouse model. Arthritis Rheumatol. 2015;67(2):454-464.
33. Finley LWS, Carracedo A, Lee J, et al. SIRT3 opposes reprogramming of cancer cell metabolism through HIF1α destabilization. Cancer Cell. 2011;19(3):416-428.
34. Arra M, Swarnkar G, Ke K, et al. LDHA-mediated ROS generation in chondrocytes is a potential therapeutic target for osteoarthritis. Nat Commun. 2020;11(1):3427.
35. Gao J, Feng Z, Wang X, et al. SIRT3/SOD2 maintains osteoblast differentiation and bone formation by regulating mitochondrial stress. Cell Death Differ. 2018;25(2):229-240.
36. Denu RA. SIRT3 enhances mesenchymal stem cell longevity and differentiation. Oxid Med Cell Longev. 2017;2017:5841716.
37. Li Q, Wang H, Zhang J, et al. Deletion of SIRT3 inhibits osteoclastogenesis and alleviates aging or estrogen deficiency-induced bone loss in female mice. Bone. 2021;144:115827.
38. Ho L, Wang L, Roth TM, et al. Sirtuin-3 promotes adipogenesis, osteoclastogenesis, and bone loss in aging male mice. Endocrinology. 2017;158(9):2741-2753.
39. Gastel N v, Carmeliet G. Metabolic regulation of skeletal cell fate and function in physiology and disease. Nat Metab. 2021;3(1):11-20.